Energy Technology & Environmental Science

Electrolytic Study of Pineapple Peel Derived Porous Carbon for All-Solid-State Supercapacitors

Prashant Dubey,[a, b] Vishal Shrivastav,[b, c] Mandeep Singh,[a, b] Priyanka H. Maheshwari,*[a, b] Shashank Sundriyal,*[a] and Sanjay R. Dhakate[a, b]

Biowaste derived carbon materials are recently gaining attention owing to their high specific surface area (SSA) and decent electrical conductivity. Herein, pineapple peel derived porous carbon nanosheets have been synthesized at different activation temperatures (PP-600, PP-700 and PP-800). This shows its high SSA along with hierarchal pore size distribution that makes it a suitable electrode material for supercapacitors. Further, the electrochemical performance of the as prepared electrode material was carried out in three different electrolytes viz. acidic (1 M H_2SO_4), basic (6 M KOH) and neutral (1 M Na_2SO_4) and among them 1 M H_2SO_4 electrolyte shows superior electrochemical performance. Furthermore, PP-800 electrode material displayed highest specific capacitance of 368.8 F/g in 1 M H_2SO_4 electrolyte, which is much higher when tested and compared in 6 M KOH (34 F/g) and 1 M Na_2SO_4 (102.7 F/g) electrolytes at a constant current density of 1 A/g. Additionally, symmetrical solid-state supercapacitor was fabricated utilizing PP-800 electrode material and PVA gel electrolyte, that rendered remarkable energy density of ~43 Wh/kg at a high-power density of ~1 kW/kg. The as fabricated PP-800//PP-800 device displayed an extraordinary cycle life exhibiting capacitance retention of 83% after 10000 ultra-long charge-discharge cycles.

1. Introduction

In the quest of meeting the soaring demands of energy due to growing population of the world, energy storage devices especially supercapacitors or ultra-capacitor prove to be a promising solution. Supercapacitors have various advantages like high power density, rapid charge/discharge rate, high columbic efficiency and very long life-time etc. Due to these advantages, supercapacitors have found applications in wide range of devices which includes portable electronic devices,[1,2] hybrid electric vehicles,[2,3] regenerative braking system and many more.[4–6] However, low energy density of supercapacitors restricts its use in energy backup devices. Supercapacitors can be categorized into electrical double layer capacitor (EDLC) and psuedocapacitor depending on their charge storage mechanism. This mechanism of charge storage in EDLC is based on the generation of oppositely charged double layer at negative and positive electrodes. On the other hand, the energy storage mechanism of psuedocapacitor involves faradaic redox reactions at the surface of electrode. However, inferior cycle life and poor electrical conductivity limit the practical applications of psuedocapacitors.

Generally, EDLC relies on the adsorption of electrolyte ions on the active electrode material's surface possessing large specific surface area. Notably, the performance of EDLC predominantly depends on the choice of electrode material. The electrode material with high SSA and appropriate pores compatible with the electrolyte ions are the demanding factors for EDLC applications.[7,8] For this purpose, carbon materials have emerged as the suitable electrode material owing to its large specific surface area, non-toxicity, chemical inertness, stability at high temperature, low coefficient of thermal expansion etc. A wide range of carbon materials like carbon nanotubes, activated carbon, graphene, carbide derived carbon, and carbon nanofibers etc. have been engineered in the recent years.[9–12] Among these materials, activated carbon turned out to be the most promising electrode material due to its highly porous nature and hierarchical pore size distributions, decent electrical conductivity, and large SSA etc. However, the high cost and harsh conditions required to synthesize conventional activated carbon have made researchers to think of other environmental-friendly and cost-effective synthesis methods.[13] Recently, biowaste precursors have been utilized to derive highly porous activated carbon for variety of energy applications. To date various biowaste precursors such as agricultural waste, forest waste, human and animal waste have been utilized to derive activated carbon for EDLC electrode fabrication.[8,14–16]

Pineapple (Ananas comosus) is one of the most commonly used fruits in the world, however its peel is of no economic value and like other wastes creates problem of disposal. The

[a] P. Dubey, M. Singh, Dr. P. H. Maheshwari, Dr. S. Sundriyal, Dr. S. R. Dhakate
Advanced Carbon Products and Metrology Department,
CSIR-National Physical Laboratory (CSIR-NPL),
New Delhi 110012, India
E-mail: hedap@nplindia.org
sundriyalshank@gmail.com
[b] P. Dubey, V. Shrivastav, M. Singh, Dr. P. H. Maheshwari, Dr. S. R. Dhakate
Academy of Scientific and Innovative Research (AcSIR),
Ghaziabad, 211002, India
[c] V. Shrivastav
CSIR-Central Scientific Instruments Organization (CSIR-CSIO),
Sector 30 C, Chandigarh, 160030, India;
Supporting information for this article is available on the WWW under https://doi.org/10.1002/slct.202103034

constituents of pineapple peel are cellulose (~19%), hemicellulose (~22%), lignin (~5%), glucose (~3.1%), fructose (~3.4%) and sucrose (~5.2%), which makes it a rich source of carbon. However, preparing the activated carbon for energy applications requires the generation of appropriate pores, since they influence the diffusion of ions in the electrode material, which in turn determines the ion storage capacity of the supercapacitor device. Many researchers have derived hierarchical porous activated carbon from biowaste precursors. For instance, Tian et al. utilized bamboo as a biowaste precursor to synthesize activated carbon showing hierarchical bee-hive like morphology.[17] The as synthesized bamboo derived hierarchical activated carbon displayed excellent performance as a supercapacitor electrode rendering high power density of 26000 W/kg at a decent energy density of 6.1 Wh/kg. Similarly, Huang et al. prepared an AC from pig bone for supercapacitor application.[18] For this study, pig bone was firstly calcined at 400 °C and then chemically activated at 800 °C that resulted into high SSA and hierarchical pore size distribution. The as synthesized material achieved high specific capacitance of 185 F/g at 0.05 A/g and beside this it also displayed good specific capacitance of 130 F/g even at a high current density of 100 A/g.

Activated carbon (AC) with controllable pore size distribution is the demanding factor for potential supercapacitor electrodes. In this study, we have presented a preparation of pineapple derived AC at different temperatures viz 600 °C, 700 °C and 800 °C to study the effect of activation temperature on the properties of material. These materials have been utilized as a positive electrode in a 3-electrode system in different nature of electrolytes viz. acidic (1 M H_2SO_4), basic (6 M KOH) and neutral (1 M Na_2SO_4). Remarkable electrochemical performance of the electrode material in 1 M H_2SO_4 electrolyte encouraged us to fabricate the solid-state symmetrical supercapacitor device utilizing PP-800 as both positive and negative electrode, which has rendered an extraordinary energy density of ~43 Wh/kg at an ultra-high power-density of ~1 kW/kg.

2. Results and discussion

KOH activation at different temperatures preceded by hydrothermal carbonization was employed to synthesize pineapple peel derived activated carbon (PP-600, PP-700 and PP-800). Hydrothermal pre-carbonization route introduces pores and defects (due to heteroatoms) in the material which is further distributed via KOH activation. Various characterizations such as, morphological, pore size distribution etc. confirms the formation of high-performance activated carbon. The schematic for the preparation of pineapple peel derived AC is given below in Figure 1.

2.1. Physicochemical properties of the pineapple peel derived activated carbon

Figure 2a shows the XRD spectra of PP–T samples prepared at varying temperatures (600, 700 and 800 °C). All the samples possess the characteristic peak of carbon at around 22–24° corresponding to the (002) plane of graphite.[19,20] The width of the peaks suggests the turbostratic structure of all the samples. This implies that the as synthesized activated carbon samples are composed of randomly oriented graphitic micro-crystallites as shown in table1 in which the crystallite size decreases with increasing activation temperature. This unusual behaviour of the carbon materials is because of the presence of KOH, which works to expand the carbon sheets and doesn't allow the orientation despite of the high temperature treatment. However, the effect of increasing heat treatment is clearly visible for samples PP-700 and PP-800 which shows the onset of peak at around 42–43° corresponding to (100) plane of graphite. However, the broad nature of the peak doesn't promise any long-range ordering even in the carbon plane.

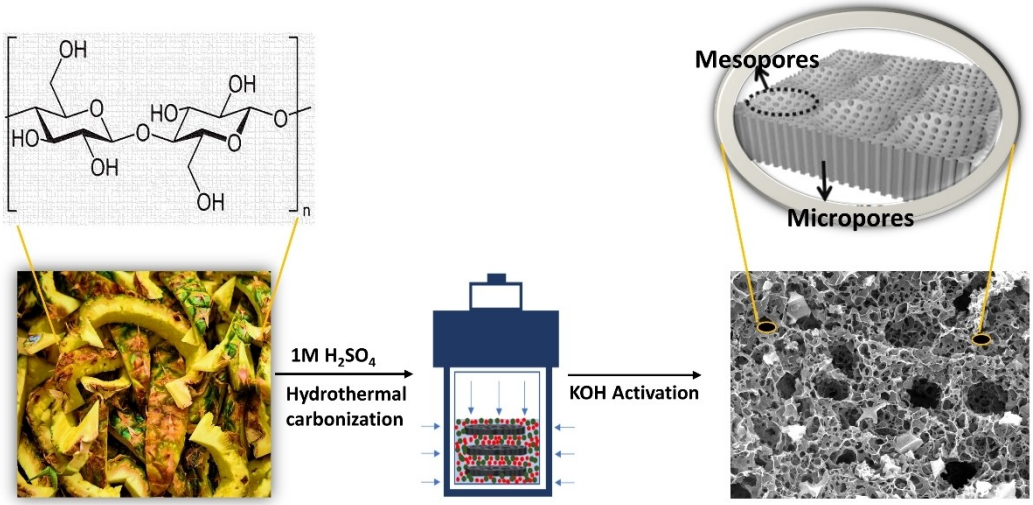

Figure 1. Schematic for the synthesis of highly porous pineapple peel derived activated carbon (PP-600, PP-700 and PP-800) using hydrothermal pre-carbonization and KOH activation approach. Partly adapted with permission from reference.[17] Copyright (2015) Royal Society of Chemistry

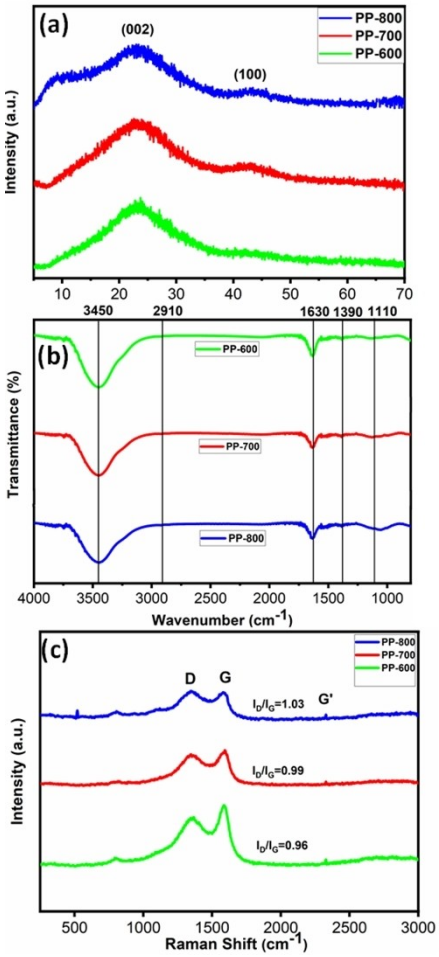

Figure 2. Physicochemical characterization of PP-600, PP-700 and PP-800 samples: (a) XRD spectra, (b) FTIR spectra, and (c) Raman spectra.

■■Dear author, please mention Table 1 in the text.■■

Besides this, FTIR of all PP–T samples were analysed at room temperature in the wavenumber range from 500 to 4000 cm^{-1}as given in Figure 2b. It is evident from the spectra that functional groups are present in all the samples. The band at 3400–3450 cm^{-1}represents the O–H vibration that is because of the stretching of surface -OH groups or the adsorbed water molecules onto the samples.[21] Small peaks at 2900–2920 cm^{-1} are assigned to the vibrations of C–H bonds. The peak observed at 1610–1634 cm^{-1} is allocated to the presence of carbonyl group and C=C stretching.[22,23] In addition, a small peak at 1390 $cm^{-1}$is ascribed to the overlapping of C–O stretching vibration while the broad peak at 1118–1080 cm^{-1}represents the C=O stretching vibrations.[23,24]

Table 1. Crystallite size of PP-600, 700 and 800 samples using XRD analysis.

Materials	(hkl)	2θ (degree)	d-spacing (nm)	FWHM (radian)	Crystallite size (nm)
PP-600	002	23.5	0.379	0.223	6.67
PP-700	002	23.2	0.385	0.224	6.46
PP-800	002	22.5	0.394	0.235	6.27

The Raman spectra of the samples is shown in Figure 2c. All the samples (PP-600, 700 and 800) possess two peaks at around 1350 cm^{-1} and 1580 cm^{-1} which corresponds to the D and G bands respectively. Among them, G band originates due to the presence of in-plane sp^2 carbon while the D band indicates the existence of defects in the material.[24,25] Also, the I_D/I_G ratio was found to be high for all the samples i.e.,0.96, 0.99, 1.03 for PP-600, 700 and 800 respectively. The slight increase in the I_D/I_G ratio with increasing activation temperature is probably due to the introduction of surface functionalities as confirmed from the FTIR data. These surface functionalities provide pseudocapacitive behaviour to the material which enhances its overall electrochemical performance. The sample PP-600 shows a hump at 2700 cm^{-1}that corresponds to G′ peak resulting in the stacking of some of graphitic planes. This G′ hump becomes sharper with increasing heat treatment due to the presence of KOH which hampers orientation in c- direction. The Raman analysis is in line with the XRD data.

XPS analysis was also used to evaluate the surface bonding of the PP-800 material. Figure 3a shows the survey scan. Only peaks corresponding to carbon, oxygen, nitrogen, and sulphur were discovered, confirming the purity of the material. In addition, Figure 3b-**3 d** shows the high resolution XPS for C1s, N1s, and O1s. Notably, C=O (289.9 eV), C=C (284.4 eV), C–O/C–N (286.9 eV), and are all present in the deconvoluted spectra of C1s. These characteristics mainly confirms the formation of activated carbon. Furthermore, O1s and N1s have also been deconvoluted, revealing distinct surface bonding.

BET analysis was carried out for the determination of SSA and pore size distribution (PSD) respectively of the as produced pineapple peel derived activated carbon samples. Figure 4a shows the BET N_2 adsorption-desorption isotherm of the PP-600, PP-700 and PP-800 samples exhibiting typical type I (microporous characteristics) and type IV (mesoporous characteristics) adsorption-desorption behavior, which indicates the coexistence of micropores and mesopores.[26] Below the relative pressure of 0.01, the steep uptake of the curve corresponds to the presence of micropores whereas above 0.01 relative pressure, the adsorption of gases indicates the mesopores.[19,27] Between relative pressure (0.4–0.9), hysteresis loop (H4) is observed indicating narrow slit-like pores with extensive size distribution.[26,28] The activation temperature influences the surface area of the samples. The SSA calculated for PP-600, 700 and 800 samples are 542, 1115 and 1643 m^2/g respectively.

Figure 4b shows the BJH plot for pineapple peel derived activated carbon samples that indicates the hierarchical distribution of meso and micropores with increase in mesoporous volume with increasing activation temperature. The average pore width is found to be 13.4, 14.4 and 15.2 nm for PP-800, PP-700 and PP-600 respectively. Furthermore, for in depth interpretation of micropores, NLDFT method is also employed to assess the pore size distribution of PP-800, PP-700 and PP-600 which is shown in Figure 4c, S1 (a) and S1 (b). The average pore width is found to be 1.273 nm for PP-800. It is well known that the highly porous nature and hierarchical PSD

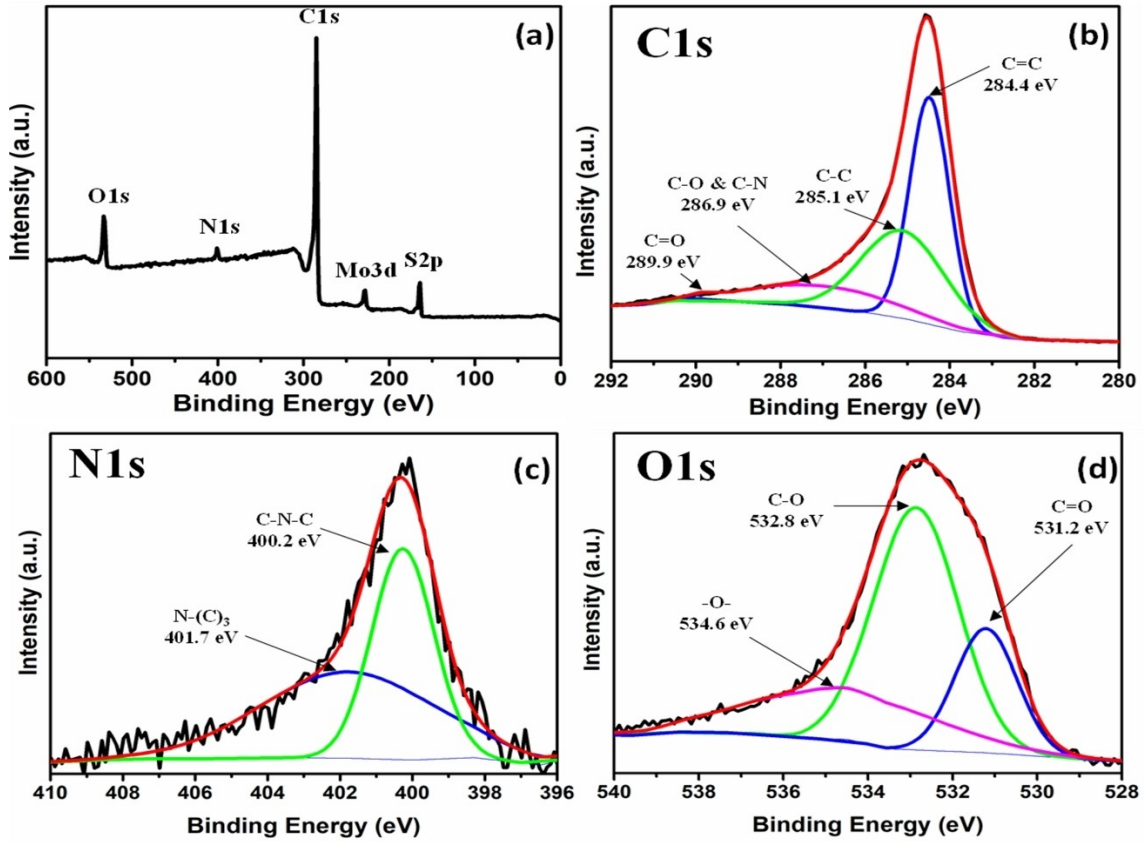

Figure 3. XPS analysis of PP-800 sample: (a) Survey scan, (b) C1s, (c) N1s, and (d) O1s.

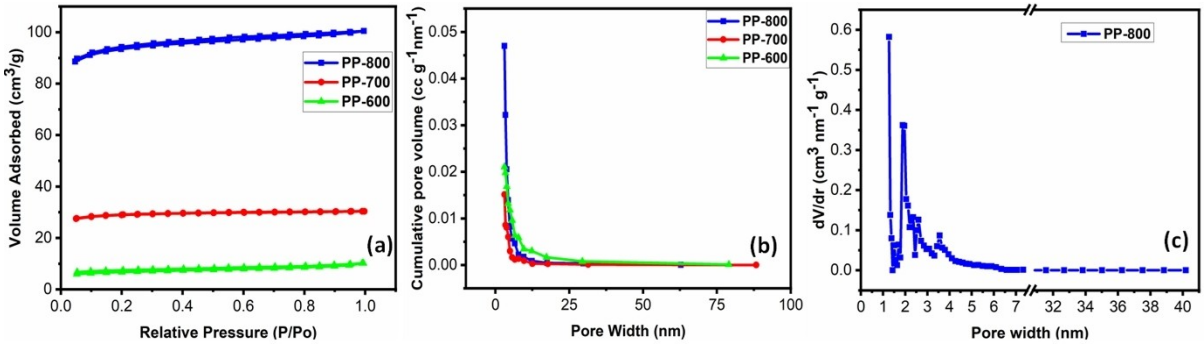

Figure 4. (a) BET N_2 adsorption-desorption isotherms, (b) BJH PSD plot of PP-600, 700 and 800 samples, and (c) NLDFT plot of PP-800 sample.

of the material allows greater access of pores of the active electrode materials to the electrolyte ions. Higher SSA and narrow PSD of PP-800 sample is advantageous for enhancing the specific capacitance, cycle life, power and energy density of SCs.

Surface morphology of the as prepared PP-800 material was characterized through FESEM, TEM along with EDS mapping which is shown in Figure 5 (a–i). From the FESEM images of the material shown in Figure 5(a–d), it was found that the sample possesses interconnected sheet-like structure which is probably due to the hydrothermal pre-carbonization step. Such morphology facilitates the rapid transport of electrolyte ions thus facilitating ideal electrode-electrolyte interaction along the surface, which could be beneficial for high performance supercapacitor. The images clearly show an interconnected porous structure with mesopores/micropores. At a high temperature of 800 °C, KOH breaches within the thin layers that facilitates the complete splitting of layers into thin sheets,[29] and generates open spaces for extensive range of pores. Further, TEM images provided the comprehensive structural information of PP-800. As depicted in Figure 5e and 5f, TEM images of the PP-800 sample demonstrate the layered type

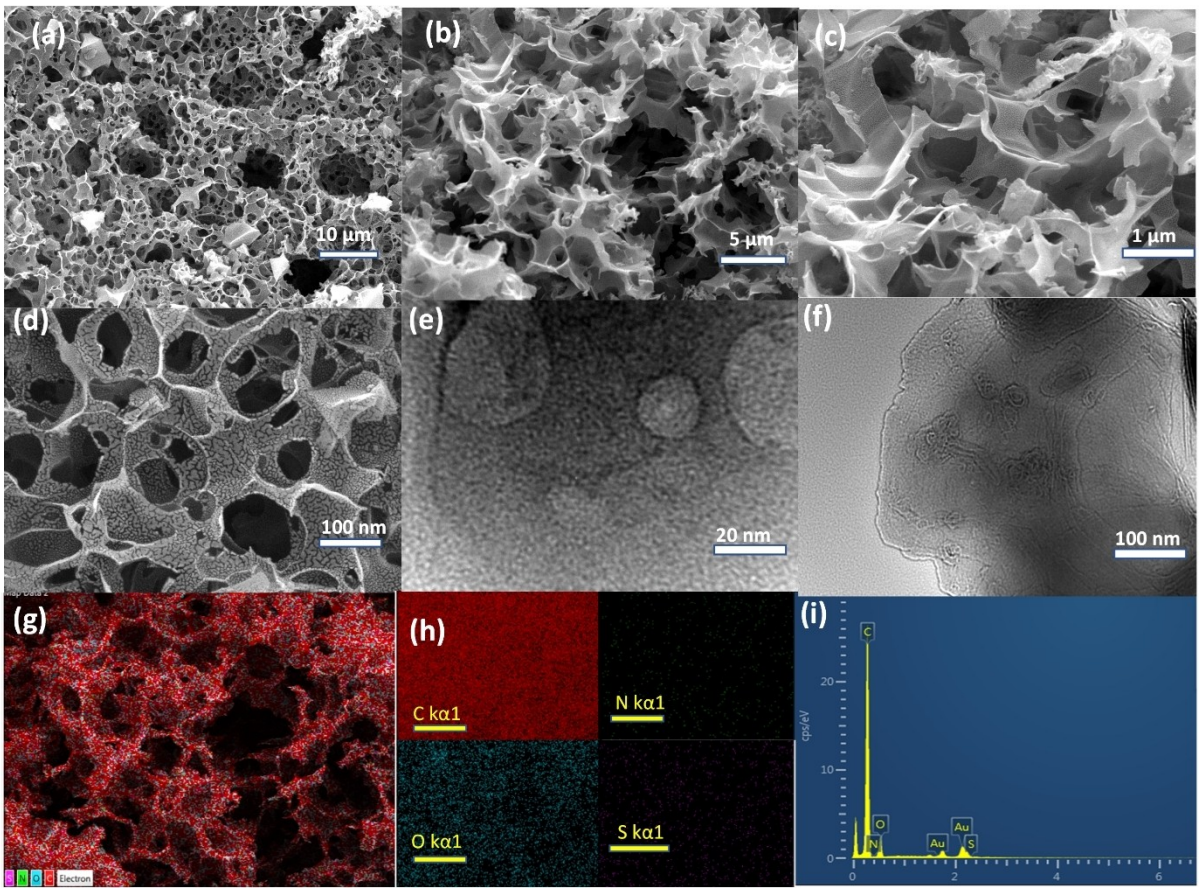

Figure 5. Morphological and elemental characterization of PP-800 sample: (a), (b), (c), and (d) are FESEM images at different magnification, (e) and (f) are TEM images, (g) elemental mapping of all the elements in PP-800, (h) elemental mapping of carbon (C), sulphur (S), Nitrogen (N) and oxygen (O) in PP-800, and (i) EDS elemental characterization of PP-800

morphology of the carbon frameworks with the existence of numerous pores within the layers which facilitates fast-electron charge transfer. Fast electrolyte transfer and easy adsorption will be aided by these pores. Micropores can serve as ion-buffering reservoirs throughout electrochemical testing and mesopores helps in facilitating the low transport resistance paths for ions into the electrode material and hence speed up the charge/discharge mechanism.

Figure 5(g &h) showed the elemental mapping of the material which confirms the presence of three different types of material i.e., carbon, sulphur, nitrogen and oxygen. Heteroatoms such as oxygen provide an extra redox activity during charge-discharge process. Further its electronegativity may facilitate fast electron transport and hence provide an extra electrical conductivity.[30] The sample shows no sign of impurity elements as shown in Figure 5(i) that displayed the percentage of different elements present in the material. As obvious from EDS graph, the material is mostly composed of Carbon. The presence of Sulphur in the sample may be attributed to the hydrothermal pre-treatment of pineapple peel with sulphuric acid during the pre-carbonization step. These findings were further corroborated via CHNSO elemental analysis which revealed that PP-800 comprises of Carbon (85.44%), Oxygen (12.84%), Nitrogen (0.56%), and Sulphur (1.16%) which is depicted in Table ST 1 of SI.

2.2. Electrochemical study of the pineapple peel derived activated carbon electrodes

Owing to the superior properties of PP-800 material, it was chosen to be further evaluated for its electrochemical performance by CV, EIS and GCD techniques in a 3-electrode system. Further, their electrochemical performance is compared in three different electrolytes viz.1 M H_2SO_4 (acidic), 1 M Na_2SO_4 (neutral), and 6 M KOH (basic). The concentration of the electrolyte solution was kept according to the previous reported literature.[17,19,31] Firstly, CV was performed at constant scan rate of 50 mV/s for PP-800 electrode with three electrolytes (as shown in Figure 6a) to determine the working potential window of the electrode. Working potential of the electrode has been evaluated by taking the potential difference between the point of stable potential (open circuit potential, OCP) and initial potential of steep increase in current indicating the decomposition of electrolyte. In this case, working potential window was found to be 1 V for both 1 M H_2SO_4 and 1 M Na_2SO_4 electrolytes while 0.7 V for 6 M KOH. From the CV curve,

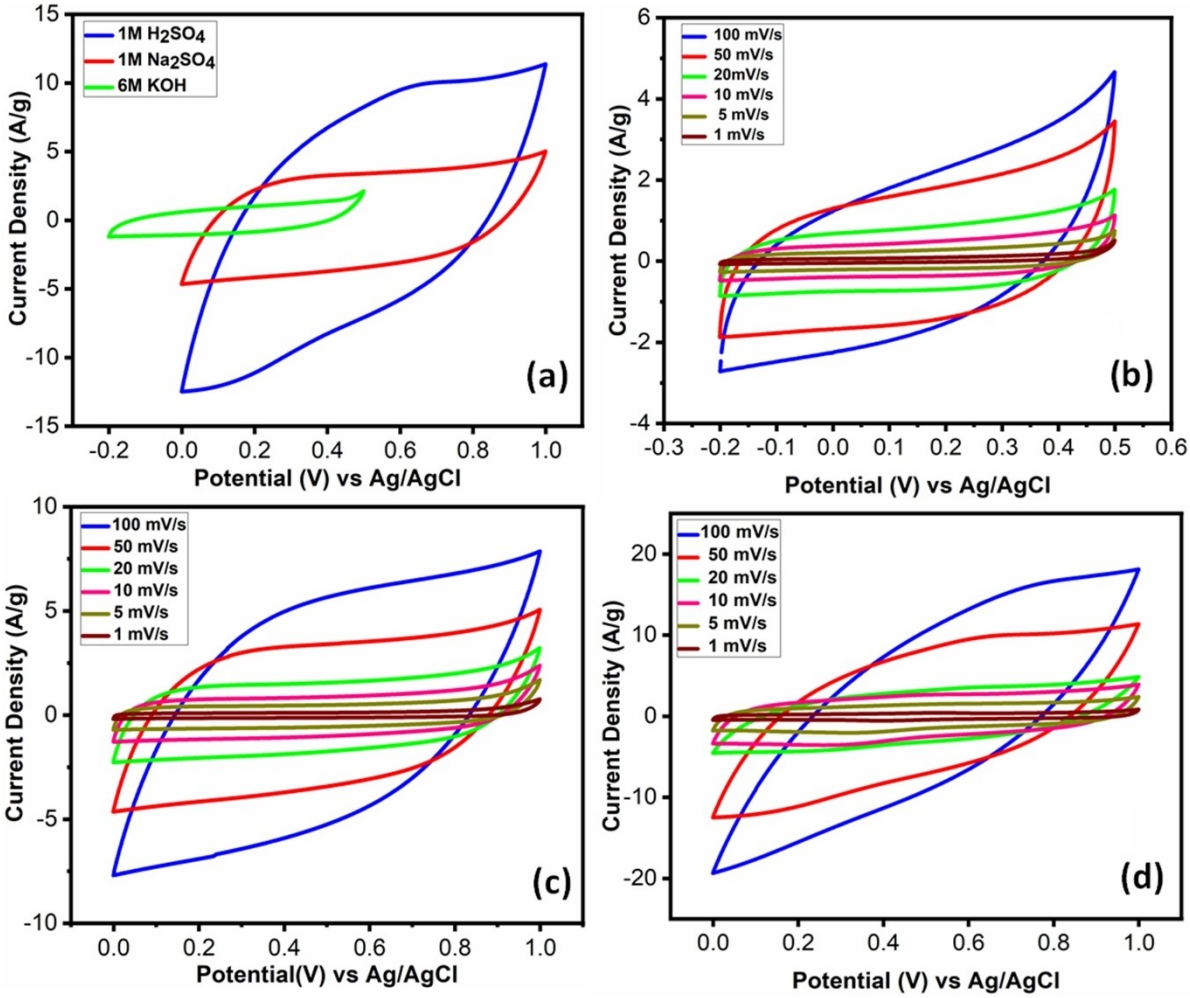

Figure 6. Electrochemical comparison of PP-800 electrode in different electrolyte system (a) CV comparison at 50 mV/s scan rate; CV at varying scan rates ranging from 1 to 100 mV/s for (b) 6 M KOH (c) 1 M Na_2SO_4 and (d) 1 M H_2SO_4.

it is evident that the area under the CV curve is found to be highest for 1 M H_2SO_4 electrolyte in comparison to 1 M Na_2SO_4 and 6 M KOH electrolytes.

The specific capacitance determined using CV analysis is 147.8 F/g in 1 M H_2SO_4 electrolyte, which is much higher than 27.5 F/g and 62.1 F/g achieved for 6 M KOH and 1 M Na_2SO_4 electrolytes respectively. In addition, the CV curves of PP-800 electrodes in three different electrolytes was also carried out at varying scan rates to investigate the energy storage mechanism. Figure 6b, c and d show the CV curves of PP-800 electrode at scan rates varying from 100 to 1 mV/s using different electrolytes viz. 6 M KOH, 1 M Na_2SO_4 and 1 M H_2SO_4, respectively. For 1 M H_2SO_4 electrolytes, PP-800 electrode material achieved specific capacitance values of 352, 279, 244.5, 190, 147.8 and 105.8 F/g at scan rate of 1, 5, 10, 20, 50 and 100 mV/s respectively. The specific capacitance via CV curves is calculated using Eq.1 of SI. All the CV curves of PP-800 electrode at different scan rates shows similar quasi-rectangular shape with no additional oxidation or reduction peaks. This indicates the formation of electric double layer (EDL) across the pineapple peel derived activated carbon (PP-800) surface which confirms the EDLC characteristic of PP-800 electrode. Owing to the presence of micro-and mesopores in the PP-800 electrode material, it maintains a perfect rectangular behavior (EDLC characteristic) even at higher scan rates.[32,33] Notably, charge storage mechanism of EDLC involves desorption and adsorption of electrolyte ions on the electrode and thus no chemical reaction is involved. High specific surface area and hierarchical pores in PP-800 material significantly enhances the adsorption of electrolyte ions, which further results in high energy density and superior power density. PP-800 electrode also demonstrates similar EDLC behavior in 6 M KOH, and 1 M Na_2SO_4 electrolytes. However, due to the difference in their ionic mass, slightly different CV curves (semi- rectangular shape) are observed in 6 M KOH and 1 M Na_2SO_4 electrolyte solution.[34,35]

GCD curves within the same potential difference as optimized earlier by CV measurements were also observed, which provides more accurate determination of the efficiency of PP-800 electrode in different electrolyte. Figure 7a shows the GCD curves comparison for PP-800 electrode using 6 M KOH,

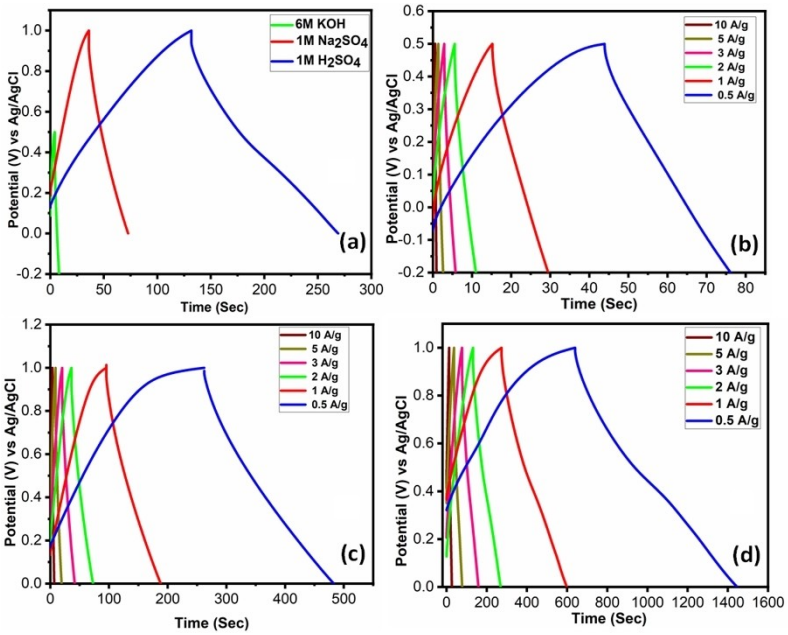

Figure 7. Electrochemical analysis for the evaluation of capacitive behavior of PP-800 electrode: (a) GCD profiles at constant current density of 2 A/g in different electrolytes (6 M KOH,1 M Na_2SO_4 and 1 M H_2SO_4); GCD at varying current densities for (b) 6 M KOH, (c) 1 M Na_2SO_4, (d) 1 M H_2SO_4

1 M Na_2SO_4 and 1 M H_2SO_4 electrolyte solution. The specific capacitance was evaluated from GCD profile using equation 2 of SI. From GCD analysis, at constant current density of 2 A/g the PP-800 electrode yielded the specific capacitance of 26.4 F/g, 83.5 F/g and 328 F/g in 6 M KOH, 1 M Na_2SO_4 and 1 M H_2SO_4 electrolytes respectively. The higher specific capacitance of PP-800 electrode in 1 M H_2SO_4 in comparison to 6 M KOH and 1 M Na_2SO_4 electrolytes is probably due to high mass loading and large solvation radius of potassium and sodium ions of respective electrolytes. This in turn might restrict the diffusion of ions inside the electrode material during charging and discharging process. On the other hand, high drift velocity and lower ionic mass of the H^+ ion facilitates the diffusion of ions inside the electrode material.[36,37] Figure 7b, c and d show GCD profiles of PP-800 electrode from 10 A/g to 0.5 A/g in different electrolyte system viz.6 M KOH, 1 M $Na_2SO_4$and 1 M H_2SO_4, respectively. Similar symmetrical linear charge-discharge curves with minimal voltage drop were observed in all the GCD profiles of all the electrolytes. These symmetrical and linear GCD profiles also indicate the ideal EDLC characteristics, thereby confirming the high performance of as synthesized PP-800 electrodes. Also, even at higher current densities, triangular GCD profiles are observed which signifies high columbic efficiency of PP-800 electrodes.

The specific capacitance using GCD plots is calculated using Eq.2 of SI. PP-800 electrode displayed high specific capacitance of 368.8 F/g in 1 M H_2SO_4 electrolyte at 1 A/g, which is much higher on comparison to specific capacitance of PP-800 in 6 M KOH (34 F/g) and 1 M Na_2SO_4 (102.7 F/g) electrolytes. High specific surface area and mesoporous characteristic of PP-800 electrode material results in high specific capacitance. In addition, high specific capacitance is also an outcome of smaller voltage drop which signifies lower equivalent series resistance of PP-800 electrode in 1 M H_2SO_4 electrolyte solution. Furthermore, lower specific capacitance is observed at higher current densities due to the much higher voltage drop.

In addition, Figure S2(a) of supporting information (SI) shows the CV analysis comparison of three different electrode materials activated at different temperatures (PP-600, 700 and 800) at a constant scan rate using 1 M H_2SO_4 electrolyte which clearly reveals that PP-800 electrode shows superior electrochemical performance than PP-700 and PP-600 electrodes. This is due to the high specific surface area and large number of meso/micro pores distribution of the PP-800 material as compared to their PP-700 and PP-600 material counterparts. GCD curves at constant current density for PP-600, PP-700 and PP-800 also verify this statement and PP-800 displayed higher charge/discharge time (Figure S2(b) of SI).

Further, Figure S2(c) of SI shows the plot of specific capacitance wrt different scan rates for all the electrode materials (PP-600, 700 and 800) in 1 M H_2SO_4 electrolyte system, which clearly shows that specific capacitance decreases constantly with increasing scan rate. This is due to the insufficient time available for the electrolyte ions for entire electrode material at high scan rates. This leads to lower capacitance value while at lower scan rates electrolyte ions can reach out to every possible accessible pore and hence results in high specific capacitance values.[38,39] The same trend of inverse characteristics has been observed in the Figure S2(d) of SI which shows the plot of specific capacitance wrt varying current densities for (PP-600, 700 and 800) electrode material in 1 M H_2SO_4 electrolyte solution. Beside this, the trends of specific capacitance wrt different scan rates and current densities for three different electrolytes is also given in Figure S3 (a) and (b)

of SI. Furthermore, Figure S4 (a) and (b) of SI shows the CV and GCD curves of current collector (graphite sheet).

EIS is an appropriate technique for evaluating the internal resistance experienced by the electrode material and also the resistance presents between electrode and electrolyte. Nyquist plot of PP-800 electrodes is recorded at a potential of 10 mV within a frequency ranging from 10 kHz-0.1 Hz for the determination of equivalent series resistance (R_s) and the charge transfer resistance (R_{ct}). The above discussed properties of the as-prepared PP-800 electrode material can be explained via Nyquist plot based on two regions i.e., high and low-frequency regions. Here, the starting point illustrates the electrode's ESR (equivalent series resistance) value (R_s), that comprises the resistance of the current collector, electrolyte resistance, and electrode material resistance while the low frequency region corresponds to the ideal capacitor (or capacitive) behavior.[40] Figure S5 of SI depicts the Nyquist plot of PP-800 electrode materials in different electrolytes for R_s and R_{ct} evaluation. From Nyquist plot, R_s is equivalent to the length of the x-axis from the starting point whereas R_{ct} in the high frequency region is equivalent to the diameter of semicircle. The low R_s value of 1.2 Ω/cm^2 and R_{ct} value of 0.13 Ω/cm^{2}is observed for PP-800 electrode in 1 M H_2SO_4 electrolyte that shows its higher conductivity than in 1 M Na_2SO_4 (R_s = 5.4 Ω/cm^2& R_{ct} = 0.20 Ω/cm^2) and 6 M KOH (R_s = 8.3 Ω/cm^2& R_{ct} = 0.22 Ω/cm^2) electrolytes. It is also corroborated from GCD results, in which the potential drop is lower in 1 M H_2SO_4 electrolytes than that of other electrolytes. On the other hand, higher values of R_s and R_{ct} for 1 M Na_2SO_4 and 6 M KOH electrolyte may be attributed to the large mass of sodium and potassium ions which may lead to the increased solvation radius and hence face higher impedance while entering into the pores of PP-800 and hence lead to the lower conductivity.

As it is clear from the CV and GCD investigations, PP-800 electrode rendered high values of specific capacitance and long cyclic life. High SSA and combination of micro and meso pores in the PP-800 electrode material are the reasons for its excellent performance. Amongst the three electrolytes (1 M H_2SO_4, 1 M Na_2SO_4 and 6 M KOH), 1 M H_2SO_4 electrolyte solution gives superior results. However, to understand the clear picture of the performance of PP-800 active electrode material, full device study is necessary for PP-800 electrode materials in 1 M H_2SO_4 electrolytes.

2.3. Electrochemical performance study of PP-800//PP-800 electrode based solid-state symmetrical supercapacitor

Owing to the promising electrochemical performance of the PP-800 electrode material in three electrode system in 1 M H_2SO_4 electrolyte, we fabricate a symmetrical supercapacitor device utilizing PP-800 electrode as both cathode and anode. PP-800//PP-800 based symmetrical solid-state device was fabricated using PVA-1 M H_2SO_4 polymer gel electrolyte sandwiched between two P-800 electrodes. Firstly, the primary step was to select the potential of symmetrical supercapacitor device. For this, CV and GCD analysis at varying potential window was carried out which is shown in Figure 8a and b respectively. From these analyses, it is found that the PP-800// PP-800 based solid-state symmetrical supercapacitor device has been operational upto 2 V. Therefore, it is concluded that the

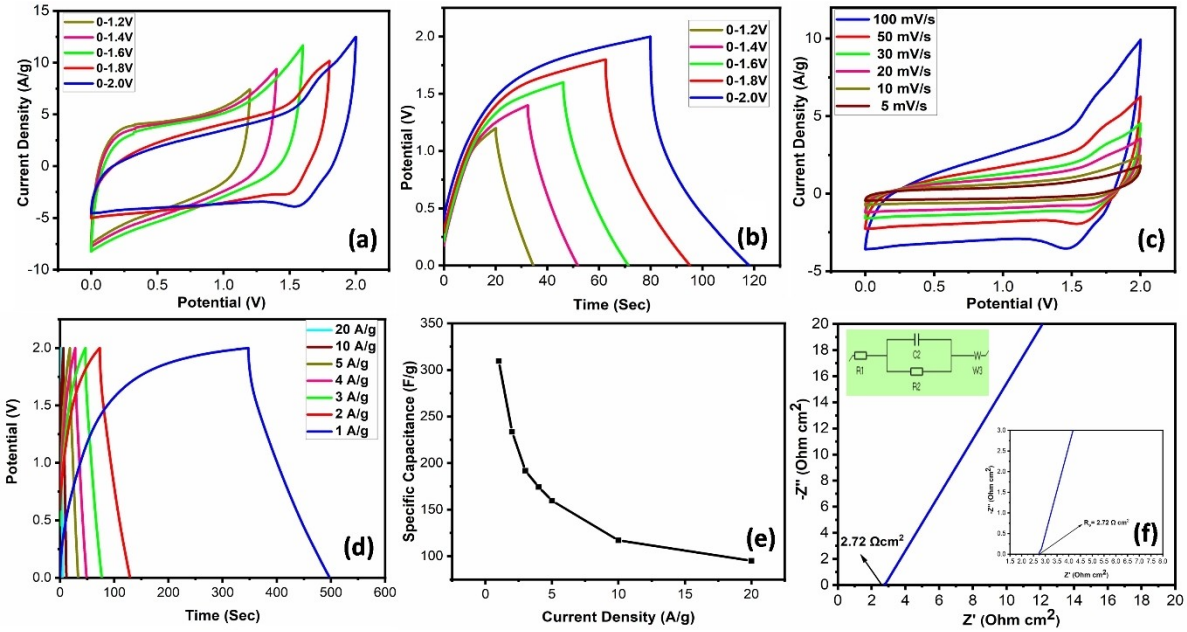

Figure 8. Electrochemical performance of PP-800//PP-800 solid-state symmetrical supercapacitor device: (a) CV at constant 50 mV/s scan rate with varying potential window, (b) GCD profiles at 2 A/g with varying potential window, (c) CV curves at scan rates varying from 100 to 5 mV/s at potential window of 0–2 V, (d) GCD profile at current densities ranging from 20 to 1 A/g, (e) plot of specific capacitance wrt different current densities, and (f) Nyquist plot with inset of its magnified plot and equivalent circuit.

as fabricated symmetrical device was optimized for potential window of 2 V (0.0–2.0 V).

The as assembled PP-800//PP-800 symmetrical supercapacitor device was tested in two electrode electrochemical cell system. CV, GCD and EIS analysis were performed for the determination of its specific capacitance, power & energy density, and ESR. CV curve was evaluated at varying scan rates ranging from 1–100 mV/s. From the CV curves of PP-800//PP-800 device as shown in Figure 8c, it is concluded that no oxidation and reduction peaks are present and the CV curves resembles the EDLC characteristics however there is some deviation from traditional rectangular EDLC behaviour. Based on this observation, it can be specified that electric double layer (EDL) has formed on the surface of PP-800 electrode. Also, the slight variation from the typical rectangular plot of EDLC is also a positive sign indicating rapid ionic transport owing to mesopores present in PP-800 active electrode material.[41] It is also observed that at a high scan rate of 100 mV/s or even at low scan rates of 5 mV/s, the CV curves are nearly rectangular, thereby confirming high power capability even at high scan rates and make them superior over batteries.

Moreover, for better interpretation of PP-800//PP-800 device, GCD analysis were performed with current densities varying from 10 to 0.5 A/g (as shown in Figure 8d). the curves show that, PP-800//PP-800 device displayed regularly symmetric GCD curves at high as well as low current densities which indicates the ideal electric double layer capacitive behaviour of the device. Therefore, the as fabricated symmetric PP-800//PP-800 SC device displayed high specific capacitance of 309.7 F/g at a current density of 1 A/g. The variation of specific capacitance of the device with varying current densities and scan rates has been given in Figure S6 of SI and Figure 8e respectively.

EIS study is utilized for determining the equivalent series resistance (ESR) for the symmetrical supercapacitor device. Figure 8f shows Nyquist plot of PP-800//PP-800, from which it was observed that findings of CV and GCD data are in good agreement with EIS measurements. At high frequency range, no semi-circular curve was observed in the Nyquist plot, which indicates that minute charge transfer resistance persists for the device. Moreover, for the symmetrical PP-800//PP-800 supercapacitor devices, ESR value was recorded to be 2.72 Ωcm^{-2}which is equivalent to starting point of the straight line at high frequency range.

In addition to above electrochemical parameters, power and energy density are two vital terms of any fabricated SC that governs its practical application as energy storage device and it was calculated from equation 3 & 4 of SI. For this, variation of energy density as a function of power density (generally known as Ragone plot) is reported in Figure 9a. From this graphical data, it is observed that PP-800//PP-800 symmetrical supercapacitor device achieved highest energy density of 43 Wh/kg at a high-power density of ~1 kW/kg. Furthermore, it is evident from the Ragone plot that with increasing power density, the energy density decays slowly. However, decent energy density of 13.2 Wh/kg is retained even at a very high-power density of 23.5 kW/kg, which demonstrate the remarkable performance of PP-800//PP-800 symmetrical supercapacitor device. Beside this, the stability of material is also a major parameter which needs to be analysed to claim the high-performance of the as fabricated device. For this, we have demonstrated the variation of columbic efficiency and capacitance retention as a function of cycle number in Figure 9b. The PP-800//PP-800solid-state symmetrical supercapacitor device displayed an extraordinary cyclic stability while retaining 83% capacitance even after 10000 GCD cycles. Additionally, 96% of coulombic efficiency after 10000 cycles indicates the excellent ability of PP-800 electrode material for supercapacitor device.

Highly porous structure, high specific surface area of PP-800 material are the main reasons for the exceptional electrochemical performance of PP-800 symmetrical supercapacitor. The electrochemical performance comparison of PP-800//PP-800 symmetrical supercapacitor device with the other reported

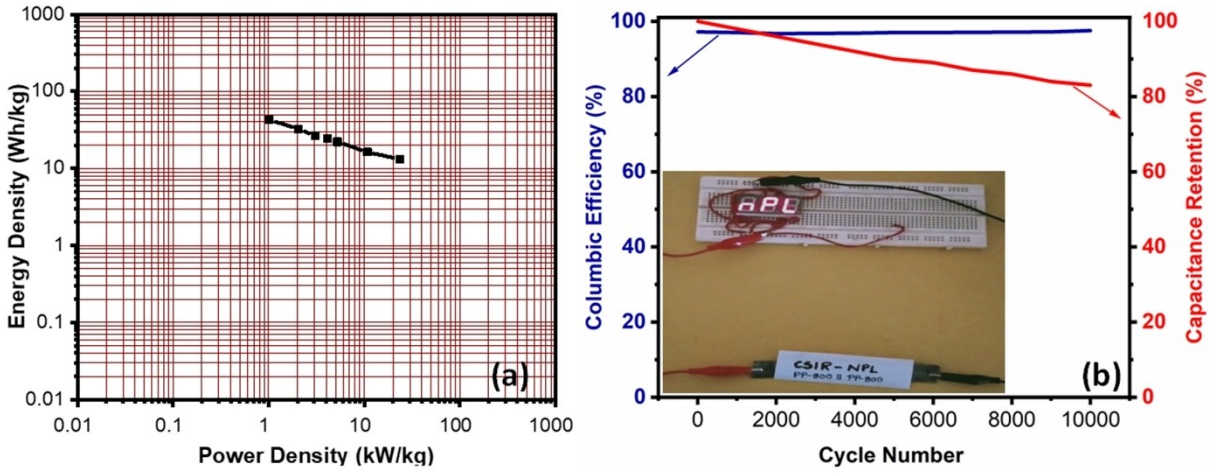

Figure 9. Electrochemical performance of PP-800//PP-800 solid-state symmetrical supercapacitor device: (a) Ragone plot, (b) columbic efficiency and capacitance retention for 10000 charge-discharge cycles at a current density of 20 A/g along with the inset of glowing of LCD display.

Table 2. Electrochemical performance comparison of pineapple peel derived porous carbon-based supercapacitor with other biowaste derived carbon-based supercapacitors.

Biowaste precursor-based supercapacitor device	Electrolyte	Specific capacitance (F/g)	Current Density (A/g)	Energy density (Wh/kg)	Power density (W/kg)	Reference
Bamboo waste// bamboo waste	6M KOH	146	0.2	9.5	25	[17]
Sword bean shell derived carbon// sword bean shell derived carbon	1 M H_2SO_4	264	1	12.5	100	[42]
Walnut shell//Walnut shell	2M KOH	137	1	21	424	[43]
Corn bract//Corn bract	1M H_2SO_4	295.6	0.5	26.3	404	[44]
Kusha grass derived carbon// kusha grass derived carbon	6M KOH	218	0.7	19.3	277.92	[45]
N-doped wood fibres// N-doped wood fibres	6M KOH	345	0.5	7.92	250	[46]
Soyabean dreg derived carbon// Soyabean dreg derived carbon	Na_2SO_4 gel	207	0.5	22	450	[47]
Helianthus annus//helianthus annus	1M Na_2SO_4	271	1	23.3	450	[48]
Office paper waste derived carbon// office paper waste derived carbon	1M H_2SO_4	99.5	0.5	31	380	[49]
Lemon peel derived carbon// Lemon peel derived carbon	1M H_2SO_4	106	0.2	11.84	361.8	[50]
PP-800//PP-800	**1 M H_2SO_4**	**309.5**	**1**	**43**	**1015**	**This Work**

symmetrical supercapacitor device using various biowaste derived activated carbon materials is given in Table 2 below.

3. Conclusion

In summary, pineapple peel has been successfully transformed into activated carbon via hydrothermal pre-carbonization and KOH activation route at different temperatures (600 °C, 700 °C and 800 °C). Structural characterization displayed the formation of meso and microporous AC with high SSA. Activated carbon synthesized at 800 °C showed better results than the synthesized products at 700 °C and 600 °C in terms of specific surface area and porous network. In addition, pineapple peel derived activated carbon at 800 °C displayed high specific capacitance in 1 M H_2SO_4 electrolyte. The unsatisfactory performance of as prepared electrode while employing 6 M KOH and 1 M Na_2SO_4 electrolytes may be attributed to the incompatible interactions of the corresponding electrolytes ions and the pores of active electrode material. The as fabricated PP-800//PP-800 solid-state symmetrical supercapacitor device renders remarkable high energy density of 43 Wh/kg at a decent power density of ~1 kW/kg with exceptional cycle life. Also, even at high power density of 23.5 kW/kg, it displayed energy density of 13.2 Wh/kg which is comparable to the commercially available activated carbon supercapacitor devices.

Supporting Information Summary

Experimental details on materials, synthesis methods, material characterization and electrochemical characterizations are given in Supporting Information. In addition, equations for evaluation specific capacitance, energy density and power density are also provided in the Supporting Information.

Credit author statement

Prashant Dubey has performed the experiments and performed electrochemical characterizations of various electrodes. Mandeep Singh and Vishal Shrivastav contributed in the study of solid-state symmetrical supercapacitor devices. Prashant Dubey and Dr. Shashank Sundriyal also prepared the first draft of the manuscript. Vishal Shrivastav also contributed in the optimization of various electrolytes. Dr. Sanjay R Dhakate contributed in data interpretation and discussion. Dr. Priyanka H. Maheshwari edited the various drafts of the manuscript, supervised the project and throughout discussion. Dr. Shashank Sundriyal conceptualized, supervised and executes the project and corrected various drafts of the manuscript.

Acknowledgments

Prashant Dubey, Mandeep Singh and Vishal Shrivastav gratefully acknowledges their research fellowships received from the CSIR, DST and UGC, India respectively. Dr. Shashank Sundriyal acknowledges the CSIR for awarding Nehru Science Post-Doctoral Fellowship (HRDG/CSIR-Nehru PDF/EN, ES & PS/EMR-1/02/2019). The authors would like to thank Director, NPL for providing the necessary research facilities and permission to publishing results.

Conflict of Interest

The authors declare no conflict of interest.

Keywords: Biowaste · Carbon · Charge transfer · Pineapple · Supercapacitor

[1] W. Raza, F. Ali, N. Raza, Y. Luo, K. H. Kim, J. Yang, S. Kumar, A. Mehmood, E. E. Kwon, *Nano Energy* **2018**, *52*, 441–473.
[2] S. Banerjee, B. De, P. Sinha, J. Cherusseri, K. K. Kar, *Handbook Nanocomp. Supercap. Mat. I: Springer* **2020**, 341–350.

[3] A. S. Veerendra, M. R. Mohamed, P. K. Leung, A. A. J. Shah, *Int. J. Green Energy* **2021**, *18*, 128–143.
[4] P. Sharma, V. Kumar, *J. Electron. Mater.* **2020**, 1–13.
[5] X. Liang, G. Long, C. Fu, M. Pang, Y. Xi, J. Li, W. Han, G. Wei, Y. Ji, *Chem. Eng. J.* **2018**, *345*, 186–95.
[6] M. Cossutta, V. Vretenar, T. A. Centeno, P. Kotrusz, J. McKechnie, S. J. Pickering, *J. Cleaner Prod.* **2020**, *242*, 118468.
[7] P. Dubey, V. Shrivastav, P. H. Maheshwari, S. Sundriyal, *Carbon* **2020**, *170*, 1–29.
[8] S. Sundriyal, V. Shrivastav, H. D. Pham, S. Mishra, A. Deep, D. P. Dubal, *Resources, Conserv. Recycling* **2021**, *169*, 105548.
[9] A. Olabi, M. A. Abdelkareem, T. Wilberforce, E. T. Sayed, *Renewable Sustainable Energy Rev.* **2021**, *135*, 110026.
[10] M. Singh, A. Gupta, S. Sundriyal, K. Jain, S. R. Dhakate, *Mater. Chem. Phys.* **2021**, *264*, 124454.
[11] P. S. Kumar, P. Prakash, A. Srinivasan, C. Karuppiah, *J. Power Sources* **2021**, *482*, 228892.
[12] K. Kannan, K. K. Sadasivuni, A. M. Abdullah, B. Kumar, *Catalysts* **2020**, *10*, 495.
[13] R. Rao, C. L. Pint, A. E. Islam, R. S. Weatherup, S. Hofmann, E. R. Meshot, F. Wu, C. Zhou, N. Dee, P. B. Amama, *ACS Nano* **2018**, *12*, 11756–11784.
[14] M. S. Priya, P. Divya, R. Rajalakshmi, *Sustainable Chem. Pharm.* **2020** *16*, 100243.
[15] K. Mensah-Darkwa, C. Zequine, P. K. Kahol, R. K. Gupta, *Sustainability* **2019**, *11*, 414.
[16] G. Li, X. Wei, Y. Li, W. Mao, G. Du, J. Zhang, *ChemistrySelect* **2020**, *5*, 2008–2014.
[17] W. Tian, Q. Gao, Y. Tan, K. Yang, L. Zhu, C. Yang, H. Zhang, *J. Mater. Chem. A* **2015**, *3*, 5656–5664.
[18] W. Huang, H. Zhang, Y. Huang, W. Wang, S. Wei, *Carbon* **2011**, *49*, 838–843.
[19] Y. T. Li, Y. T. Pi, L. M. Lu, S. H. Xu, T. Z. Ren, *J. Power Sources* **2015**, *299*, 519–528.
[20] H. A. Rahman, S. X. Chin, *Sains Malays.* **2019**, *48*, 385–391.
[21] M. Aravind, M. P. Amalanathan, *Mater. Today* **2021**, *43*, 1491–1495.
[22] D. Lan, M. Chen, Y. Liu, Q. Liang, W. Tu, Y. Chen, J. Liang, F. Qiu, *J. Mater. Sci. Mater. Electron.* **2020**, *31*, 18541–18553.
[23] S. Muduli, V. Naresh, S. K. Martha, *J. Electrochem. Soc.* **2020**, *167*, 090512.
[24] I. I. Misnon, N. K. M. Zain, T. S. Lei, B. L. Vijayan, R. Jose, *Ionics* **2020**, *26*, 4081–4093.
[25] D. Yu, C. Chen, G. Zhao, L. Sun, B. Du, H. Zhang, Z. Li, Y. Sun, F. Besenbacher, M. Yu, *ChemSusChem* **2018**, *11*, 11678–1685.
[26] P. I. Ravikovitch, A. Vishnyakov, R. Russo, A. V. Neimark, *Langmuir* **2000**, *16*, 2311–2320.
[27] Y. Li, X. Ding, Y. Guo, C. Rong, L. Wang, Y. Qu, X. Ma, Z. Wang, *J. Hazard. Mater.* **2011**, *186*, 2151–2156.
[28] M. U. Rani, K. Nanaji, T. N. Rao, A. S. Deshpande, *J. Power Sources* **2020**, *471*, 228387.
[29] H. Wang, Z. Xu, A. Kohandehghan, X. Li, K. Cui, X. Tan, T. J. Stephenson, C. K. Kingondu, C. M. B. Holt, B. C. Olsen, J. K. Tak, D. Harfield, A. O. Anyia, D. Mitlin, *ACS Nano* **2013**, *7*, 5131–5141.
[30] Y. Li, S. Zhang, H. Song, X. Chen, J. Zhou, S. Hong, *Electrochim. Acta* **2015**, *180*, 879–886.
[31] M. D. Mehare, A. D. Deshmukh, S. Dhoble, *J. Mater. Sci.* **2020**, *55*, 4213-4224, 2020.
[32] C. Portet, G. Yushin, Y. Gogotsi, *J. Electrochem. Soc.* **2008**, *155*, A531.
[33] C. Lekakou, O. Moudam, F. Markoulidis, T. Andrews, J. Watts, G. Reed, *J. Nanobiotechnol.* **2011**, 2011.
[34] P. Manasa, Z. J. Lei, F. Ran, *J. Energy Storage* **2020**, *30*, 101494.
[35] S. Yang, K. Zhang, *Nanomaterials* **2018**, *8*, 181.
[36] H. Wu, X. Wang, L. Jiang, C. Wu, Q. Zhao, X. Liu, B. Hu, L. Yi, *J. Power Sources* **2013**, *226*, 202–209.
[37] N. Maile, S. Shinde, R. Koli, A. Fulari, D. Kim, V. Fulari, *Ultrason. Sonochem.* **2019**, *51*, 49–57.
[38] H. Yamada, H. Nakamura, F. Nakahara, I. Moriguchi, T. Kudo, *J. Phys. Chem. C* **2007**, *111*, 227–233.
[39] S. Sundriyal, V. Shrivastav, H. Kaur, S. Mishra, A. Deep, *ACS Omega* **2018**, *12*, 17348–17358.
[40] B. A. Mei, O. Munteshari, J. Lau, B. Dunn, L. Pilon, *J. Phys. Chem. C* **2018**, *122*, 194–206.
[41] Q. Liang, L. Ye, Z. H. Huang, Q. Xu, Y. Bai, F. Kang, Q. H. Yang, *Nanoscale* **2014**, *6*, 13831–13837.
[42] T. Chen, L. Luo, L. Luo, J. Deng, X. Wu, M. Fan, G. Du, W. Zhao, *Renewable Energy* **2021**, *175*, 760–769.
[43] W. Wang, J. Qi, Y. Sui, Y. He, Q. Meng, F. wei, Y. Jin, *J. Nanosci. Nanotechnol.* **2018**, *18*, 5600–5608.
[44] G. Ma, Z. Zhang, K. Sun, E. Feng, H. Peng, X. Zhou, Z. Lei, *J. Power Sources* **2016**, *330*, 219–230.
[45] G. K. Gupta, P. Sagar, S. K. Pandey, M. Srivastava, A. K. Singh, J. Singh, A. Srivastava, S. K. Srivastava, A. Srivastava, *Nanoscale Res. Lett.* **2021**, *16*, 85.
[46] F. Liu, Y. Gao, C. Zhang, H. Huan, X. Chu, Z. Xu, Z. Wiang, H. Zhang, X. Xiao, W. Yang, *J. Colloid Interface Sci.* **2019**, *548*, 322–332.
[47] Y. Zhou, J. Len, L. Xia, Q. Jheng, J. Liao, E. Long, F. Xie, C. Xu, D. Lin, *Electrochim. Acta* **2018**, *284*, 336–345.
[48] W. Zhang, B. Liu, M. Yang, Y. Liu, H. Li, P. Liu, *J. Mater. Sci. Technol.* **2021**, 2021.
[49] S. Sundriyal, V. Shrivastav, A. Kaur, P. Dubey, S. Mishra, A. Deep, S. R. Dhakate, *IEEE Trans. Nanotechnol.* **2021**, *20*, 481–488.
[50] M. D. Mehare, A. D. Deshmukh, S. J. Dhoble, *J. Mater. Sci. Mater. Electron.* **2021**, *32*, 14057–14071.

Submitted: August 26, 2021
Accepted: October 29, 2021

FULL PAPERS

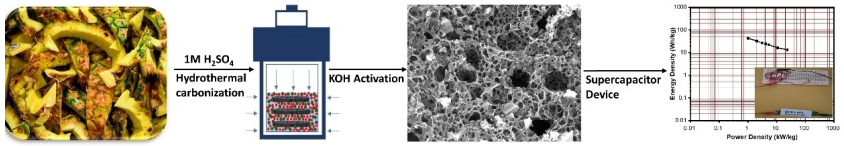

P. Dubey, V. Shrivastav, M. Singh, Dr. P. H. Maheshwari, Dr. S. Sundriyal*, Dr. S. R. Dhakate*

1 – 12

Electrolytic Study of Pineapple Peel Derived Porous Carbon for All-Solid-State Supercapacitors

Pineapple peel was choosen as biowaste precursor to derive higly porous activated carbon via simple hydrothermal carbonization followeed by KOH activation technique. The as obtained product have heirarchical pore size distribution and high specific surface area as confirmed via FESEM, TEM and N_2 adsorption-de-sorption characterization. Highly porous pineapple peel derived activated carbon then utilized to fabricate an all-solid-state symmetrical supercapacitor device which shows tremendous performance.

Author Contributions

P.D. Methodology:Lead; Writing – original draft:Equal
V.S. Investigation:Supporting; Methodology:Supporting
M.S. Formal analysis:Supporting; Investigation:Supporting
P.M. Data curation:Supporting; Resources:Lead; Supervision:Equal; Visualization:Equal; Writing – review & editing:Supporting
S.S. Conceptualization:Lead; Data curation:Equal; Formal analysis:Lead; Supervision:Equal; Writing – original draft:Equal; Writing – review & editing:Equal
S.D. Resources:Lead; Writing – review & editing:Supporting